Controlled Modification of Erbium Lifetime by Near-Field Coupling to Metallic Films

New Journal of Physics
The open-access journal for physics

Controlled modification of erbium lifetime by near-field coupling to metallic films

Nanfang Yu[1], **Alexey Belyanin**[2], **Jiming Bao**[1,3] **and Federico Capasso**[1,4]

[1] Harvard School of Engineering and Applied Sciences, Harvard University, Cambridge, MA 02138, USA
[2] Department of Physics, Texas A&M University, College Station, TX 77843, USA
E-mail: capasso@seas.harvard.edu

New Journal of Physics **11** (2009) 015003 (15pp)
Received 28 June 2008
Published 30 January 2009
Online at http://www.njp.org/
doi:10.1088/1367-2630/11/1/015003

Abstract. Systematic measurements of the photoluminescence lifetime of the 1.54 μm transition of erbium implanted at different energies in SiO_2 films with different metallic overlayers are reported. The lifetime shows a strong reduction up to a factor of 20 with decreasing distance between the erbium and the metal overlayer. The reduction of lifetime is mainly due to a near-field interaction between the erbium ions and the metal overlayers through generation of surface plasmon polaritons at the metal/SiO_2 interface and direct generation of heat in the metal. These experiments combined with rigorous theoretical modeling demonstrate that a high degree of control over the radiative properties of erbium can be achieved in erbium-implanted materials in a wide range of implantation energies. The experiments also allow us to determine the radiative efficiency of erbium in bulk SiO_2.

Contents

[3] Present address: Department of Electrical and Computer Engineering, University of Houston, Houston, TX 77204-4005, USA.
[4] Author to whom any correspondence should be addressed.

1. Introduction

Erbium is a rare-earth ion of paramount technological importance for optics and optoelectronics. Its $^4I_{13/2}$–$^4I_{15/2}$ optical transition falls into one of the silica fibers transmission windows near 1.5 μm. Erbium-doped fibers are the backbone of optical communications [1]. Erbium-doped or -implanted crystals, thin films and nanostructures can be used for fabrication of solid-state lasers, amplifiers, modulators and other optoelectronics devices [2]–[4].

In bulk crystals, the lifetime of the 1.54 μm transition is of the order of 15 ms and is dominated by spontaneous emission. It is well known that both the spontaneous emission rate and the separation between energy levels are affected by the presence of boundaries and interfaces with other materials (substrate, air, cavity mirrors, etc) that change the spatio-temporal structure of the electromagnetic (EM) modes via boundary conditions, see, e.g. [5], reviews [6]–[8] and references therein. The most obvious way to accomplish this is to place an atom or any quantum oscillator in a high-Q, low-volume cavity [9]. This will definitely modify the properties of all radiated modes and lead to drastic changes in the quantum dynamics of an atom. Typical experimental settings involve single atoms and molecules in a microwave or optical cavity. Recent studies of this cavity-QED effect in solids with application to new devices include quantum-well and quantum-dot excitons in microcavities with Bragg mirrors, microdisk cavities and photonic crystal cavities, see e.g. [10]–[14]. Another possibility is to provide a strong resonant coupling of an atomic oscillator with a given normal EM mode, for example with the surface plasmon mode [14]–[17].

It is less obvious that the dynamics of a quantum dipole can be significantly modified in the presence of any conducting or dielectric surface, far from any resonances with eigenmodes of a medium and in the absence of mode-selective environment. If the interface with a conducting or dielectric medium is located in the near zone of an atom, i.e. at a distance R much less than the optical transition wavelength, the level shift and modification of the spontaneous decay rate can be quite dramatic [18]–[24]. In this case the influence of a boundary on the radiative decay rate is mainly due to a semiclassical London–van der Waals self-action (not due to EM vacuum fluctuations). This is essentially a semiclassical effect in a sense that the EM field may be treated classically, while the atom should be treated quantum-mechanically. Therefore, it can be adequately described by the change in the total EM reaction field acting on a quantum dipole. This approach was shown to provide accurate quantitative results in the seminal series of papers by Chance *et al*; see their review in [24].

At small distances from the interface, it is the quasi-electrostatic near field that makes the main contribution to the total EM reaction field. This near-field-dominated EM reaction can be intuitively viewed as a quasi-electrostatic near field created by an image dipole at the position of a real dipole. However, this intuitive picture shows a good quantitative agreement with rigorous calculations only in the limit $R \to 0$, or at any R when the substrate is a perfect conductor or a non-absorbing dielectric [6–8, 25, 26]. In the latter two cases, the quasi-static part of the EM reaction field is shifted in phase by exactly $\pi/2$ with respect to the dipole oscillations. As a result, the work done by the near field over the optical dipole oscillations of an atom is equal to zero and the only effect on the spontaneous emission lifetime is due to the far-field radiation reaction, i.e., due to the modification of EM radiation modes emitted into the far zone.

When the imaginary part ε_2'' of the dielectric constant of a substrate is not equal to zero or infinity, the near field contributes also to the spontaneous decay rate, and this contribution can be dominant under certain conditions. The underlying physical mechanism is the

near-field-mediated energy transfer between the oscillating quantum dipole and the dissipative substrate. For a dielectric or semiconducting substrate the dominant channel of the energy transfer in the visible or near-infrared spectral range is the direct Joule dissipation of the near field in the substrate. In the vicinity of metals the dissipation of energy of dipole oscillations can also be mediated by excitation of surface or interface plasmons if the dipole frequency is close to the plasmon resonance.

Recently, Kalkman *et al* [16] demonstrated enhanced photoluminescence (PL) decay rate for the Er/silica glass/silver system, but the study was limited to one Er-implantation depth. The magnitude of the effect is expected to depend sensitively on the dielectric function of a given metal, the structure of the interface and its distance from atoms. Therefore, we were motivated to study the modification of the spontaneous emission decay of the 1.54 μm transition in erbium-implanted silicon dioxide films coated with different metals and at different implantation depths. We have reported in a previous publication measurements of the lifetime of Er implanted at different energies in SiO_2 film coated with Cr and Ti [27]. It was shown there that the measured lifetime agrees with modeling reasonably well. In this paper we report systematic measurements and calculations of Er lifetime for seven different metallic coatings.

Erbium can be implanted at high doses in SiO_2 with well-characterized profiles and diffuses minimally at temperatures required to anneal the implants ($\sim$950 °C). Radiative efficiency in the annealed samples is very high, between 65 and 85% as shown below. Besides the obvious motivation to understand and predict the magnitude of the spontaneous emission modification in these structures, the near-field energy transfer mechanism provides the interesting possibility of controlling the lifetime of excited electron states in active impurities or semiconducting nanostructures by varying their distance to the dissipative layer and its absorptive properties. We find the effect to be very strong, more than a factor of 20 spontaneous emission rate enhancement over the bulk value in the shallowest-implanted samples. This creates opportunities for enhancing the modulation rate and controlling the saturation nonlinearity in devices implanted or doped with erbium and other active impurities. Furthermore, our measurements allow direct determination of the radiative efficiency (quantum yield) of the 1.54 μm transition in erbium, which is a crucial parameter for Er-doped optical devices.

2. Experiments

Polished 1 μm-thick SiO_2 films on 380 μm-thick Si wafers were implanted with Er^+ ions to a fluence of 2×10^{13} ions cm^{-2} (Implant Sciences Corporation). Implantation energies 10, 20, 40, 80, 150 and 300 keV were used. Thermal annealing of the implanted wafers was performed at 950 °C in a tube furnace for 1.5 h under vacuum conditions ($\sim 1 \times 10^{-7}$ Torr) to remove implantation induced defects [27]–[29]. Dynamic secondary-ion mass spectrometry (SIMS) was used to characterize Er ion concentrations in the thermally annealed samples with different Er-implantation energies. SIMS measurements were done using a 100 nA 2 keV oxygen beam, with a beam diameter of approximately 30 μm. This beam was rastered over a 250×250 μm^2 area, and the secondary ion signal was electronically gated to the center 15% of the crater area. The measurement results are summarized in figure 1. Gaussian functions can fit the Er concentration profiles for large implantation energies reasonably well but there is some skewness in the Er concentration profiles for implantation energies 10 keV and 20 keV. For comparison, simulations were also performed to predict Er concentration profiles using the Monte Carlo package in the

Table 1. Results of SIMS experiments and SRIM simulations.

Er implantation energy (keV)	Er profile peak depth (nm) (SRIM)	FWHM of Er profile (nm) (SRIM)	Er profile peak depth (nm) (SIMS)	FWHM of Er profile (nm) (SIMS)	Peak Er concentration (at.%)
10	12.2	5.65	13.3	12.9	0.023
20	17.7	8.48	20.2	16.0	0.019
40	26.4	13.2	26.6	17.9	0.017
80	41.3	21.0	42.5	26.7	0.011
150	64.0	33.0	68.5	40.2	0.008
300	108.9	56.3	113.8	67.6	0.005

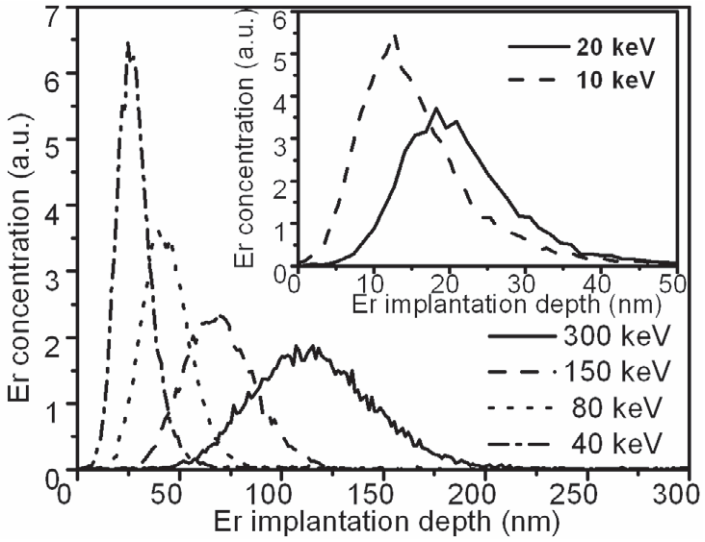

Figure 1. Measured SIMS profiles of the Er ions implanted at different energies. The curves from left to right in the figure correspond to implantation energies 40, 80, 150 and 300 keV. Inset: the left and right curves correspond to implantation energies 10 and 20 keV.

SRIM 2003 program. Table 1 summarizes and compares the results of SIMS experiments and SRIM simulations.

It is found from table 1 that the peaks of Er concentration profiles predicted by SRIM simulations agree reasonably well with SIMS experiments results: discrepancy between the two ranges from ∼5% for the deep-implantation cases to ∼10% for the shallow-implantation cases. However, there are relatively large divergences between the Er concentration profile width taken from SRIM simulations and SIMS experiments: for the deep-implantation cases discrepancies are ∼20%; for the shallow-implantation cases (10 keV and 20 keV), the full-widths at half-maximum (FWHM) of the concentration profiles measured by SIMS experiments is larger than that SRIM obtained by a factor of 2. There are several possible reasons for the discrepancies. SIMS measurements may give rise to broadened concentration profiles due to the so-called

'crater-edge effect' (milling of not only the crater bottom but also the crater sidewalls), but this effect is expected to be very small since in the SIMS experiments the secondary ion signal was electronically gated to the center of the crater area during ion milling. Thermal annealing prior to SIMS experiments is also unlikely to account for the broadening of the concentration profiles because heavy ions like Er are known to diffuse very little in SiO_2 during annealing [29]. The most probable reason turns out to be surface effects (roughness, contamination, etc), which introduce a certain degree of randomness to the starting energy of Er ions at the air/SiO_2 interface during implantations, especially for the cases of very small implantation energies such as 10 keV and 20 keV [30]. This point is supported by the skewness of the SIMS profiles for the 10 keV and 20 keV samples: ideally the concentration profile should be Gaussian for an amorphous substrate [31]. Since Monte Carlo simulations do not consider any surface effects, Er concentration profiles obtained from SIMS experiments are used for the analyses presented later in this paper.

After annealing, metal was deposited by resistive heating onto the implanted side of the sample to a thickness of $\sim$160 nm, which is optically thick compared with skin depth of Er radiation in the metal. Thermal deposition was performed using a thermal evaporator (Sharon Vacuum) at a deposition rate of 0.2–0.3 nm s^{-1} under $\sim 2 \times 10^{-7}$ Torr vacuum condition. The samples were at room temperature during deposition. Metals used in our experiments include Cr, Ti, Co, permalloy (Ni, 84 at.%, Fe 16 at.%), Cu, Ag and Au. Deposition followed annealing immediately after to minimize exposure of the samples to water vapor or any other contaminations in the air. Without this precaution, the measured PL lifetimes decrease up to 25% for the uncoated shallowest-implanted samples over several days. This is probably due to luminescence quenching defects and impurities near the sample surface: the shallowest-implanted samples with Er ions about 10 nm away from the air/SiO_2 interface are very sensitive to any change of the sample surface state.

The adhesion strength of different metals on SiO_2 is different. Cr and Ti stick well to SiO_2 due to the formation of metallic oxides at the interface. Samples coated by Cr or Ti do not exhibit PL lifetime decrease even when stored in air for a few months. Transition metals Ni, Fe and Co are similar but their adhesion strength to SiO_2 is weaker. Noble metals Cu, Ag and Au, the least reactive among these metals, adhere loosely to SiO_2, resulting in a porous metal/SiO_2 interface. This should modify the effective dielectric constant of metallic films as will be shown later in the theoretical analyses. Before PL measurements, the samples were annealed for a second time in vacuum at 110 °C for 9 h in order to reduce defects originating from grain boundaries in the metal films [32].

A schematic of the setup for Er PL lifetime measurements is shown in figure 2. Measurements were performed in ambient conditions at room temperature. Square 50 ms-long pulses from a $\lambda = 980$ nm fiber laser (JDS Uniphase) were collimated and focused into a $\sim 0.5 \times 0.5$ mm^2 area on the nonimplanted side of the samples with $\sim$10 mW peak power. The duty cycle of the pulses was about 10%. Figure 3 shows a typical PL spectrum of one sample (without metal coating) with characteristic peaks around 1.54 μm which correspond to the Er $^4I_{13/2}$–$^4I_{15/2}$ transition. The Er PL was collected through a $\lambda = 1.4$ μm long-wavelength pass filter and focused onto an InGaAs detector (Electro-Optical Systems Inc.) with a long wavelength cutoff of 1.6 μm. Time traces of PL intensity after averaging show smooth decaying tails following the excitation pulses. Typical PL decay curves in logarithmic scale are shown in figure 4. PL lifetimes are obtained by fitting with an exponential curve the initial part of the PL signal, during which the signal drops by approximately a factor of 5 from its maximum value. In

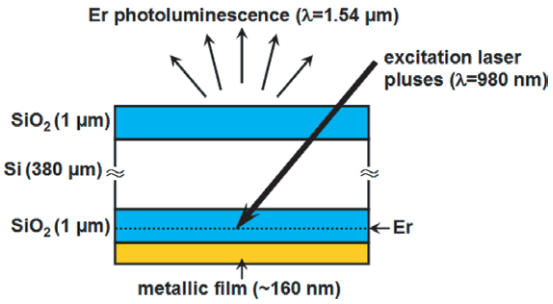

Figure 2. A schematic of the setup for Er PL lifetime measurements.

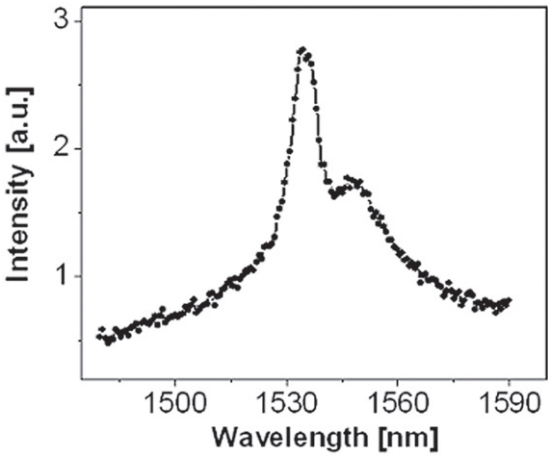

Figure 3. PL spectrum from a sample with 150 keV Er-implantation energy.

the shallowest-implanted samples, the lifetimes are not much longer than the detector response time, which is about 0.2 ms. In this case, deconvolution was used to extract the PL decay time. Experimentally, changing the excitation incident angle or power did not affect the measured lifetime.

In order to facilitate comparison with theoretical calculation, we also determined experimentally the lifetime of Er in bulk SiO_2 (bulk lifetime). The value is found to be 14.3 ± 0.3 ms. Samples for this experiment were fabricated by further depositing 1 μm SiO_2 onto the Er-implanted side of the annealed wafers (without metal coating) using plasma-enhanced chemical vapor deposition (PECVD). This is to minimize the interaction between the near field of Er ions (which extend about one wavelength away from the ion cores) and any neighboring interfaces. Measurements of the bulk lifetimes from three samples with 80, 150 and 300 keV Er-implantation energies gave very similar results of $\sim$14.3 ms. Samples with large implantation energies were chosen for this measurement because the shallowest-implanted samples are more susceptible to the influence of water vapor in the air before depositing the 1 μm-thick SiO_2. The bulk lifetime determined in our experiments is consistent with reported values from $\sim$14 ms to $\sim$17 ms [2, 28, 29]. The distribution of reported bulk lifetimes is due to different annealing conditions, which results in different nonradiative decay rates, or due to slightly different sample geometries.

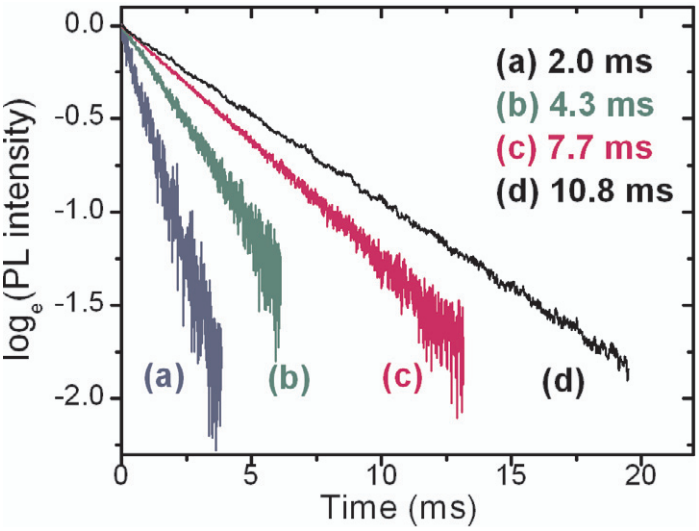

Figure 4. Erbium PL intensity decay curves for a variety of implantation energies and metal coatings: (a) Ti coated, 40 keV Er; (b) Cr coated, 80 keV Er; (c) Ti coated, 150 keV Er; and (d) Cr coated, 300 keV Er. Shown are the corresponding lifetimes. Intensities are normalized to their corresponding maxima before taking logarithm.

3. Theory and discussion

Theoretical normalized decay rates for the same implantation energies were calculated and compared with experiment according to the following procedure. First, the expression for the spontaneous decay rate of a single ion at a given distance z from a planar interface was obtained. We calculated the electric field created by an oscillating quantum dipole at its position in the host medium with real dielectric constant $\varepsilon_1 = n_1^2$ at a distance $z = z_0$ from a medium with complex dielectric constant ε_2. This field is then substituted as an external field in the Bloch equations for the quantum dipole oscillator, which gives rise to the spontaneous decay rate. The resulting expressions [25, 26] for the decay rate of a dipole with transverse and parallel orientation with respect to the interface are in exact agreement with equations (2.17) and (2.29) obtained in [24] on the basis of Hertz vectors formalism:

$$\gamma_{\mathrm{t}} = \Gamma_0^{\mathrm{rad}} \left\{ 1 - \frac{3}{2} \mathrm{Im} \left(\int_0^\infty R_{\mathrm{p}} \frac{u^3}{a_1} \exp(-4\pi n_1 a_1 z_0/\lambda) \mathrm{d}u \right) \right\}, \tag{1}$$

$$\gamma_{\mathrm{p}} = \Gamma_0^{\mathrm{rad}} \left\{ 1 + \frac{3}{4} \mathrm{Im} \left(\int_0^\infty \left[(1-u^2) R_{\mathrm{p}} + R_t \right] \frac{u}{a_1} \exp\left(-4\pi n_1 a_1 z_0/\lambda\right) \mathrm{d}u \right) \right\}, \tag{2}$$

u is the normalized wavevector and equals to k/k_1, where k_1 is the wavevector in medium 1, $\lambda = 2\pi c/\omega_0$ is the optical transition wavelength in vacuum, Γ_0^{rad} is the radiative decay rate in the bulk SiO_2;

$$R_{\mathrm{t}} = \frac{a_1 - a_2}{a_1 + a_2}, \quad R_{\mathrm{p}} = \frac{\varepsilon_1 a_2 - \varepsilon_2 a_1}{\varepsilon_1 a_2 + \varepsilon_2 a_1}, \quad a_1 = -\mathrm{i}\sqrt{1-u^2}, \quad a_2 = -\mathrm{i}\sqrt{\varepsilon_2/\varepsilon_1 - u^2}.$$

$\varepsilon_1 = 1.44^2$ is the dielectric constant of SiO_2 and ε_2 is the dielectric constant of the coating medium, i.e. the metal film. Equations (1) and (2) are exact within the semiclassical theory for a dipole located near the plain interface. They include all relevant effects such as dissipation, reflection of the total EM field and excitation of the interface plasmons. The latter effect is enhanced in the spectral range where the resonant denominator in the expression for R_p becomes small. Optical constants of bulk metals are taken from [33] for transition metals and from [34] for noble metals.

We also evaluated the effect of the interface between Si and SiO_2 located at a distance of 1 μm from the SiO_2–metal interface (see figure 2), using the 'double-interface' expressions for the decay rate derived in [24]. We found that taking this interface into account results in the change in the theoretical decay rate by at most 3%. Therefore, we neglected the Si/SiO_2 interface to simplify the subsequent calculations.

Using the distribution $f(z)$ of implanted Er ions measured in the SIMS experiments, the time dependence of the PL is found as $I(t) \propto \int f(z) \exp(-\gamma(z)t)\, dz$, where $\gamma(z)$ is the spontaneous decay for an atom at a distance z, averaged over random dipole orientations:

$$\gamma(z) = (\gamma_t + 2\gamma_p)/3. \tag{3}$$

The resulting time dependence $I(t)$ is nonexponential. The decay slows down with time in quantitative agreement with observations. In correspondence with the experimental procedure, we fitted only the initial part of the computed function $I(t)$ with an exponential dependence. The values of exponents for different metals are shown in figures 5–11 with blue filled dots. In calculating these points, dielectric constants of bulk metals were used and an abrupt interface between SiO_2 and metal was assumed.

As is seen from figures 5 and 6, for Ti and Cr the theoretical decay rates (blue dots) follow the experimental decay rates (red triangles) and are slightly higher than the latter. This is due to the fact that some fraction of the excited Er ions recombines nonradiatively by transferring the excitation energy to impurities and defects located in the immediate vicinity. Similarly to the approach applied in [23] to CdSe nanocrystals, by comparing theoretical and experimental decay rate we can extract a very important parameter: the radiative efficiency q of Er in SiO_2. In bulk SiO_2 the total measured decay rate $\Gamma_0 = 1/\tau_0 = 1/(14.3\,\text{ms})$ is the sum of its radiative and nonradiative parts: $\Gamma_0 = \Gamma_0^{rad} + \Gamma_0^{nr}$. Here, the nonradiative part is due to the nonradiative excitation transfer to immediate neighbors of the excited Er ions, which is unrelated to the radiation reaction effect. Therefore, it should remain the same after the structure is coated with a metal film. Then the total decay rate measured in our experiments in the metal-coated sample for the same implantation energy is $\Gamma = \Gamma^{rad} + \Gamma_0^{nr}$. From the last two equations for Γ and Γ_0 we calculate the radiative efficiency of Er implanted in bulk SiO_2:

$$q = \frac{\Gamma_0^{rad}}{\Gamma_0} = \frac{(\Gamma/\Gamma_0) - 1}{(\Gamma^{rad}/\Gamma_0^{rad}) - 1}. \tag{4}$$

The normalized radiative decay rate $\Gamma^{rad}/\Gamma_0^{rad}$ in (4) is calculated theoretically by fitting $I(t)$ as described above. Γ_0 and Γ in (4) are experimentally determined quantities.

Ideally, q calculated from (4) should yield the same value for all samples and implantation energies. In reality, there is some variation both from one kind of metal to another and between different implantation energies for the same metal. The former is most likely related to the quality of the interface between SiO_2 and the metal film. To eliminate this uncertainty, the data for Ti- and Cr-coated samples that have the best adhesion properties and interface quality have

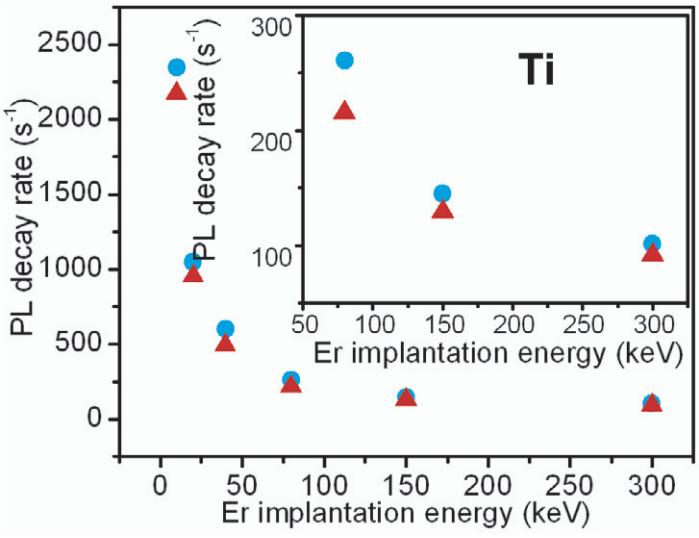

Figure 5. Er PL decay rates for samples coated with titanium. Blue dots and red triangles are calculations and experimental data, respectively. Inset: zoom-in view of the three points with the highest implantation energies. For increasing implantation energy, the relative errors of the theoretical decay rates are ±10%, ±10%, ±5%, ±4%, ±2% and ±1%; the relative errors of the experimental decay rates are ±10%, ±7%, ±5%, ±5%, ±5% and ±3%. The relative errors for other metallic coatings are quite similar as these values. The errors of the theoretical data are mainly due to an uncertainty in determining the Er-implantation depth. The latter was used for theoretical calculations. The errors in the experimental data are mainly due to the variation in the lifetimes measured in different spots across the wafer.

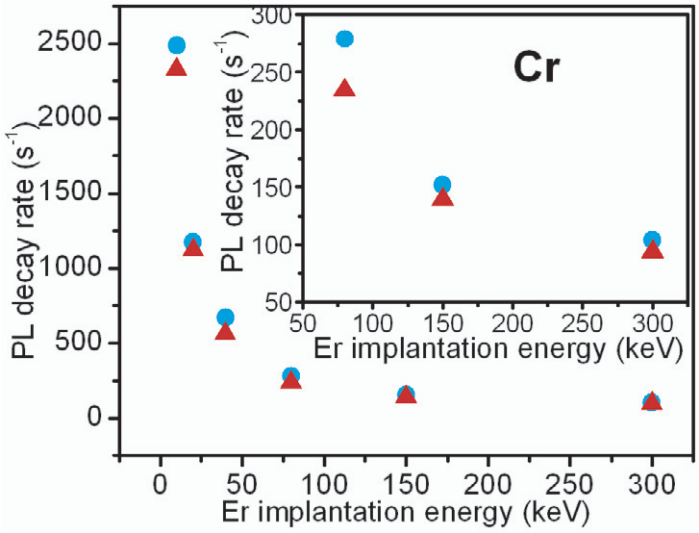

Figure 6. Er PL decay rates for samples coated with chromium. Blue dots and red triangles are calculations and experimental data, respectively. Inset: zoom-in view of the three points with the highest implantation energies.

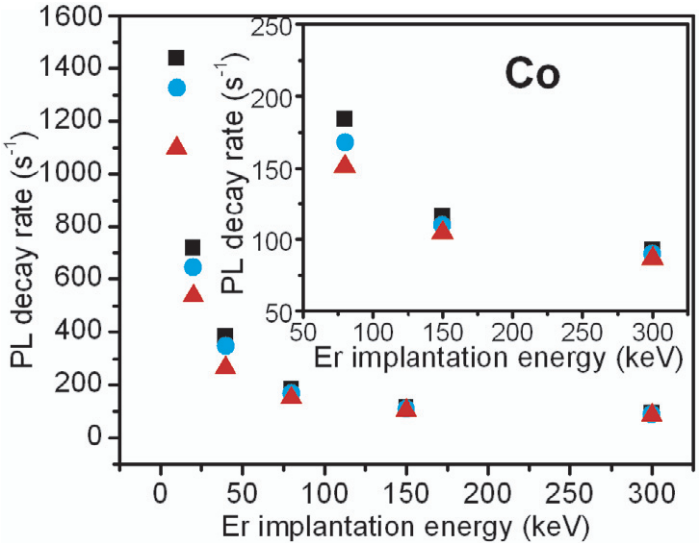

Figure 7. Er PL decay rates for samples coated with cobalt. Blue dots are calculations assuming no voids at the metal/SiO_2 interface; black squares are calculations assuming a void fraction f_v of 0.1; red triangles are experimental data. Inset: zoom-in view of the three points with the highest implantation energies.

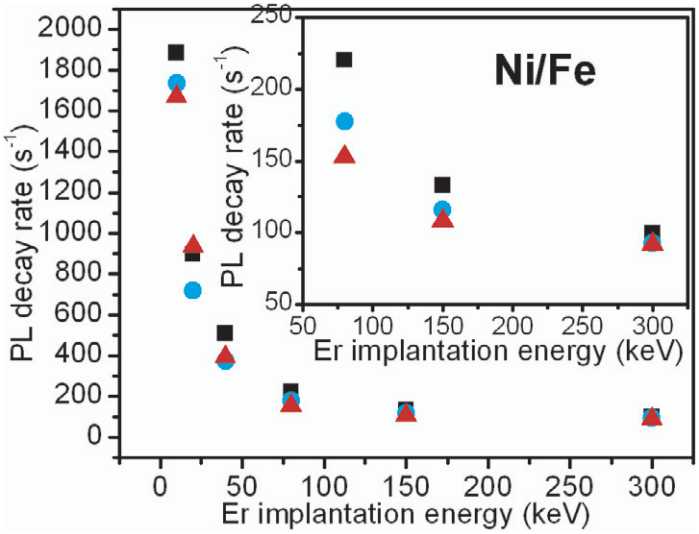

Figure 8. Er PL decay rates for samples coated with permalloy. Blue dots are calculations assuming no voids at the metal/SiO_2 interface; black squares are calculations assuming a void fraction f_v of 0.2; red triangles are experimental data. Inset: zoom-in view of the three points with the highest implantation energies.

been used. For Ti- and Cr-coated samples at six implantation energies from 10 keV to 300 keV the calculated efficiencies are summarized in columns 2 and 3 of table 2. For all samples except the Cr-coated one with the implantation energy of 20 keV the variations in the values of efficiency are within the experimental error and are consistent with the numbers reported in

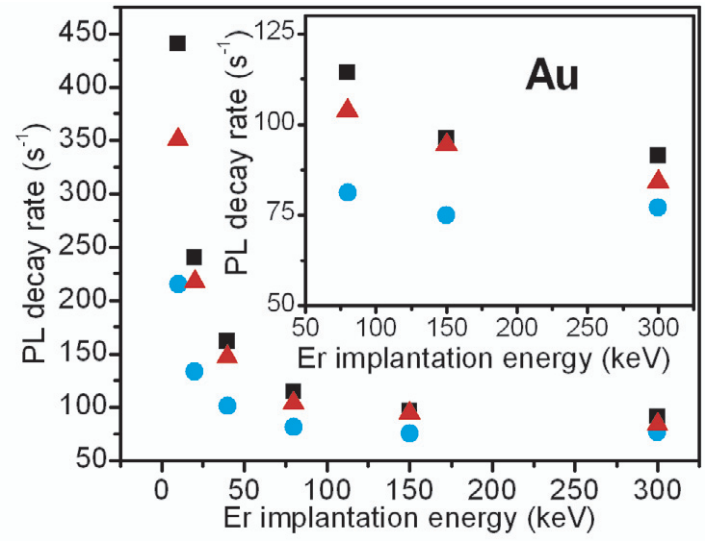

Figure 9. Er PL decay rates for samples coated with gold. Blue dots are calculations assuming no voids at the metal/SiO_2 interface; black squares are calculations assuming a void fraction f_v of 0.4; red triangles are experimental data. Inset: zoom-in view of the three points with the highest implantation energies.

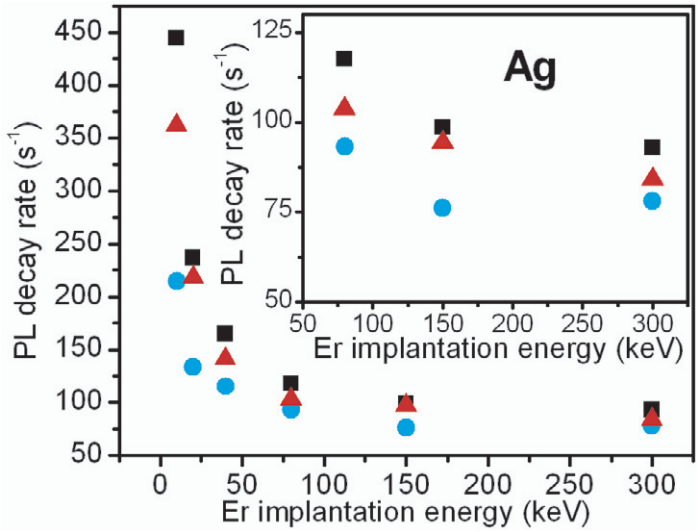

Figure 10. Er PL decay rates for samples coated with silver. Blue dots are calculations assuming no voids at the metal/SiO_2 interface; black squares are calculations assuming a void fraction f_v of 0.4; red triangles are experimental data. Inset: zoom-in view of the three points with the highest implantation energies.

the literature [1, 19, 28]. A slight decrease in radiative efficiency for the highest implantation energy of 300 keV is likely due to a stronger structural damage in the immediate vicinity of the implanted ions that persists even after proper annealing. A slight decrease in the value of q for the shallowest implants could be due to an enhanced density of quenching centers near the

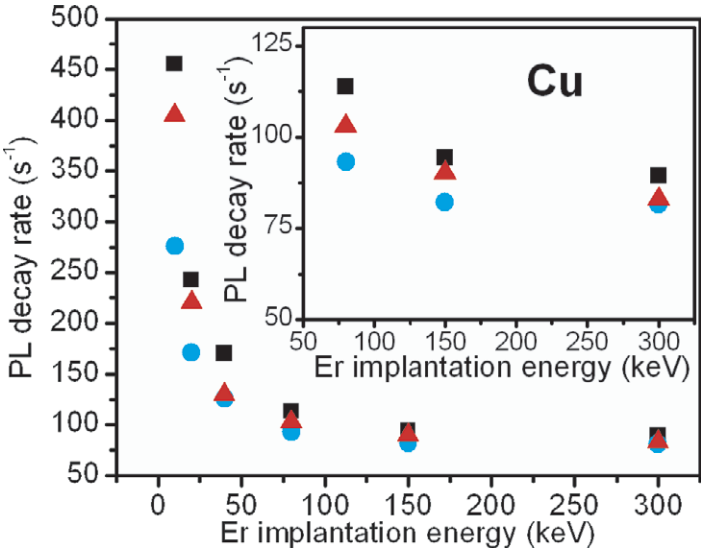

Figure 11. Er PL decay rates for samples coated with copper. Blue dots are calculations assuming no voids at the metal/SiO_2 interface; black squares are calculations assuming a void fraction f_v of 0.25; red triangles are experimental data. Inset: zoom-in view of the three points with the highest implantation energies.

SiO_2 surface [28]. In our case the hydroxyl groups of water vapor are the most likely quenching centers and they affect the shallowest-implanted samples the most [35].

For Cu-, Au- and Ag-coated samples the discrepancy between the calculations and the experimental data (blue dots and red triangles in figures 9–11) is much larger than the experimental uncertainties. Moreover, for most points the theoretical decay rates are lower than the experimental decay rates, leading to meaningless values of radiative efficiency larger than one. A probable reason for this discrepancy is poor adhesion of these metals to SiO_2, which results in the significant amount of voids in the metallic film near the metal/SiO_2 interface. In the absence of any information about the structure of the interface we will assume that the interface layer of the film (at least within the skin depth) is a microstructured isotropic mixture of bulk metal grains and voids with characteristic scale of the microstructure smaller than the wavelength of light. Then the dielectric constant ε_f of this layer can be calculated within the effective medium approximation. We will use the Bruggeman's formula [36] which seems to be a better approximation for metallic films than the Maxwell–Garnett theory [37, 38], especially when the void fraction f_v is not small [39]:

$$f_v \frac{\varepsilon_v - \varepsilon_f}{\varepsilon_v + 2\varepsilon_f} + (1 - f_v) \frac{\varepsilon_m - \varepsilon_f}{\varepsilon_m + 2\varepsilon_f} = 0, \tag{5}$$

where ε_m is the dielectric constant of bulk metal and ε_v is the dielectric constant of voids, assumed to be equal to one (air voids).

The dielectric constant of the film depends on a single parameter f_v which is unknown. However, we can use the fact that the radiative efficiency of Er in the samples covered with noble metals should be the same as in the samples covered with Ti, Cr, Co and permalloy, i.e. of the order of 70%. This should be true at least for the samples with high implantation energies

Table 2. Radiative efficiency of Er in SiO_2 derived from comparing experimental and theoretical decay rates in metal-coated samples for different implantation energies. The fraction of voids f_v used to calculate the dielectric constant of a film is indicated.

Implantation energy (keV)	Ti bulk ε	Cr bulk ε	Co $f_v = 0.1$	Permalloy $f_v = 0.2$	Au $f_v = 0.4$	Ag $f_v = 0.4$	Cu $f_v = 0.25$
10	0.72	0.75	0.75	0.88	0.76	0.78	0.87
20	0.79	0.96	0.92	1.05	0.87	0.89	0.87
40	0.79	0.82	0.62	0.73	0.84	0.75	0.60
80	0.76	0.78	0.71	0.55	0.76	0.70	0.75
150	0.79	0.85	0.74	0.61	0.93	0.96	0.83
300	0.68	0.70	0.73	0.73	0.66	0.62	0.67

in which most Er ions are far from the interface. Therefore, we can turn the problem around and find the void fraction which yields radiative efficiencies of about 70% for deep-implanted samples covered by a given metal. Then we use this void fraction to calculate the theoretical decay rate for samples with other implantation energies and repeat this procedure for all metals. The result is shown in figures 7–11 with black squares. The values of void fraction found with this procedure are $f_v = 0.4$ for Au and Ag and 0.25 for Cu films, respectively. The dielectric constants for these films are $-36.83 + 4.37i$, $-33.11 + 3.49i$ and $-41.56 + 6.23i$, respectively, where i is the imaginary unit. Obviously, they correspond to 'poorer' metals as compared with the bulk dielectric constants of $-95.57 + 10.91i$, $-86.29 + 8.70i$ and $-67.60 + 9.97i$, respectively. The void fraction is quite high especially for Au and Ag. This is most likely due to poor adhesion between the films and SiO_2. One evidence for poor adhesion is that we found that the noble metal films deposited on the sample wafers can be peeled off relatively easily. f_v determined from our experiments is comparable to previously reported values for gold films [39].

The radiative efficiencies for all implantation energies obtained using the dielectric constants for noble metal films with voids are summarized in table 2 in the last three columns. The values of q are similar to that for Ti- and Cr-coated films, indicating that the Bruggeman's model is a good fit for our films. There is a similar decrease in the radiative efficiency for samples with the highest implantation energy, indicating possible radiation damage. Two points for the implantation energy of 150 keV show the values of q that are too high: 0.93 for Au and 0.96 for Ag. This discrepancy could be a sign of light scattering by macroscopic inhomogeneities at the film interface, which is not described by the adopted model.

Samples covered with Co and permalloy films are expected to have an intermediate quality of metal/SiO_2 interface. Adopting the same procedure as for noble metal films, we arrive at a lower fraction of voids: 0.1 and 0.2, respectively. The results for radiative efficiency for these two metals are shown in columns 4 and 5 of table 2. They show a reasonable uniformity and agreement with the results for Ti- and Cr-coated samples for all implantation energies except 20 keV, for which the values of q are way too high. In fact, as can be seen from the table, for all metals the value of q at 20 keV is significantly higher than the average q. One possible explanation for this anomaly is that the actual penetration depth of Er ions at this energy is somewhat smaller than the value of 20.2 nm indicated by SIMS measurements.

4. Conclusions

Our results indicate that the decay rate of the 1.54 μm optical transition in erbium-implanted samples and optoelectronic devices can be strongly enhanced (by more than a factor of 20) in a well-controllable and predictable way by a fairly simple and straightforward procedure of metal coating. This procedure also permits direct measurements of the quantum efficiency of implanted erbium, which turns out to be quite high, in the range of 70–80%, indicating a high quality and robustness of implanted samples. It is expected that similarly strong effects with the same degree of consistency and controllability can be achieved for other rare-earth and possibly transition-metal ions that possess near-infrared transitions well shielded from the local environment. It would be interesting to study the effect for other types of interfaces, for example with a semiconductor, which would enable the possibility to manipulate the dielectric constant ε_2 via the electric current of bias. Also it is worth trying other device geometries, for example fibers, pillars, etc.

Acknowledgments

We acknowledge support from the Air Force Office of Scientific Research (AFOSR MURI on Plasmonics) and the Harvard Nanoscale Science and Engineering Center (NSEC). This work was performed in part at the Center for Nanoscale Systems (CNS) at Harvard University, a member of the National Nanotechnology Infrastructure Network (NNIN), which is supported by the National Science Foundation. CNS is part of the Faculty of Arts and Sciences at Harvard University. We would like to thank Dr Thomas Mates for his help on SIMS measurements and Dr Mariano Troccoli for helpful discussions and suggestions.

References

[1] Desurvire E 2002 *Erbium-Doped Fiber Amplifiers, Principles and Applications* (New York: Wiley-Interscience)
[2] Vredenberg A M, Hunt N E J, Schubert E F, Jacobson D C, Poate J M and Zydzik G J 1993 *Phys. Rev. Lett.* **71** 517–20
[3] Kalkman J, Tchebotareva A, Polman A, Kippenberg T J, Min B and Vahala K J 2006 *J. Appl. Phys.* **99** 083103
[4] Polman A, Min B, Kalkman J, Kippenberg T J and Vahala K J 2004 *Appl. Phys. Lett.* **84** 1037–9
[5] Purcell E M 1946 *Phys. Rev.* **69** 681
[6] Hinds E A 1991 *Adv. At. Mol. Opt. Phys.* **28** 237
[7] Agarwal G S, Gupta S D and Puri R R 1995 *Fundamentals of Cavity Quantum Electrodynamics* (Singapore: World Scientific)
[8] Meschede D 1992 *Phys. Rep.* **211** 201–50
[9] Kleppner D 1981 *Phys. Rev. Lett.* **47** 233–6
[10] Suemune I, Ueta A, Avramescu A, Tanaka S, Kumano H and Uesugi K 1999 *Appl. Phys. Lett.* **74** 1963–5
[11] John S and Quang T 1994 *Phys. Rev.* A **50** 1764–9
[12] Quang T, Woldeyohannes M and John S 1997 *Phys. Rev. Lett.* **79** 5238–41
[13] Lavallard P 1996 *Acta Phys. Pol.* A **90** 645
[14] Vahala K J 2006 *Nature* **424** 839–46
[15] Neogi A, Lee C W, Everitt H O, Kuroda T and Tackeuchi A 2002 *Phys. Rev.* B **66** 153305
[16] Kalkman J, Kuipers L, Gersen H and Polman A 2005 *Appl. Phys. Lett.* **86** 041113
[17] Kalkman J, Strohhöfer C, Gralak B and Polman A 2003 *Appl. Phys. Lett.* **83** 30–2

[18] Drexhage K H 1974 *Progress in Optics* vol 12 ed E Wolf (New York: Elsevier) p 163
[19] Snoeks E, Lagendijk A and Polman A 1995 *Phys. Rev. Lett.* **74** 2459–62
[20] Huang Z, Lin C C and Deppe D G 1993 *IEEE J. Quantum Electron.* **29** 2940–9
[21] Belyanin A A, Kocharovsky V V, Kocharovsky Vl V and Capasso F 2002 *Phys. Rev. Lett.* **88** 053602
[22] Zhang J Y, Wang X Y and Xiao M 2002 *Opt. Lett.* **27** 1253–5
[23] Brokmann X, Coolen L, Dahan M and Hermier J P 2004 *Phys. Rev. Lett.* **93** 107403
[24] Chance R R, Prock A and Silbey R 1978 *Advances in Chemical Physics* vol 37 ed I Prigogine and S A Rice (New York: Wiley) p 1
[25] Kocharovsky V V, Kocharovsky Vl V and Belyanin A A 1996 *Phys. Rev. Lett.* **76** 3285–8
[26] Belyanin A A, Kocharovsky V V and Kocharovsky Vl V 1995 *Laser Phys.* **5** 1164–70
[27] Bao J, Yu N, Capasso F, Mates T, Troccoli M and Belyanin A 2007 *Appl. Phys. Lett.* **91** 131103
[28] Polman A 1997 *J. Appl. Phys.* **82** 1–39
[29] Polman A, Jacobson D C, Eaglesham D J, Kistler R C and Poate J M 1991 *J. Appl. Phys.* **70** 3778–84
[30] Spaepen F 2007 Private communication
[31] Ohring M 2001 *Materials Science of Thin Films* (New York: Academic)
[32] Marie-Luce Thèye 1970 *Phys. Rev.* B **2** 3060–78
[33] Johnson P B and Christy R W 1974 *Phys. Rev.* B **9** 5056–70
[34] Palik E D 1985 *Handbook of Optical Constants of Solids* (New York: Academic)
[35] Yan Y, Faber A J and Waal H D 1995 *J. Non-Cryst. Solids* **181** 283–90
[36] Bruggeman D 1935 *Ann. Phys.* **24** 636–4
[37] Aspnes D E 1985 *Handbook of Optical Constants of Solids* ed E D Palik (New York: Academic)
[38] Aspnes D E, Theeten J B and Hottier F 1979 *Phys. Rev.* B **20** 3292–302
[39] Jungk G and Röseler A 1986 *Phys. Status Solidi* b **137** 117–23